Original Article
Synergistic anti-tumor effect of anti-PD-L1 antibody cationic microbubbles for delivery of the miR-34a gene combined with ultrasound on cervical carcinoma

Yun Liu[1*], Jinjun Jiang[2*], Chaoqi Liu[2,3], Wensi Zhao[4], Yao Ma[2], Zhiwei Zheng[2], Qing Zhou[1], Yun Zhao[2,3]

[1]Echo Laboratory, Department of Ultrasound Imaging, Renmin Hospital of Wuhan University, Wuhan, China; [2]Medical College of China Three Gorges University, Yichang, China; [3]Hubei Key Laboratory of Tumor Microenvironment and Immunotherapy, Yichang, China; [4]Cancer Center, Renmin Hospital of Wuhan University, Wuhan, China. *Equal contributors.

Abstract: This study explored the synergistic effect of anti-PD-L1 antibody cationic microbubbles (MBs) for delivery of the miR-34a gene combined with ultrasound in inhibiting the cervical cancer. H&E stain, TUNEL, immunohistochemistry and RT-PCR were used to detect the change of apoptosis regulatory factors, and immunofluorescence, Flow cytometry and LDH assays were applied to evaluate the changing of immunomodulatory. In this experiment the PD-L1 Ab/miR-34a-MBs were prepared successfully. The cell targeting assay showed that U14 cells were surrounded by the PD-L1 Ab/miR-34a-MBs and microbubbles had well contrast imaging capability in vivo. With the irradiation power was 1 W/cm^2 and the irradiation time was 25 s, the gene transfection efficiency was the highest using EGFP plasmid lorded microbubbles. In vivo anti-tumor assays, the PD-L1 Ab/miR-34a-MBs showed a great potential in inhibiting tumor growth with a TGI of >50%. PD-L1 Ab/miR-34a-MBs treatment enhanced the anti-tumor effect compared with that induced by PD-L1 Ab or miR-34a alone. Firstly, PD-L1 Ab/miR-34a-MBs could gather miR-34a with high-concentration aggregation and releasing around the cervical cancer, which takes a significant role in promoting apoptosis by downregulated Bcl-2 and upregulated Bax. Furthermore, combination therapy was found to augment the activation of T lymphocytes proliferation and increase CD8+ T cells infiltration, to enhance antitumor immune killing effect. The anti-PD-L1 antibody microbubbles for delivery miR-34a gene with ultrasound were considered to be a promising combination therapy regimen via initiating apoptotic mechanism of the tumor and anti-tumor immune regulation.

Keywords: Ultrasound, microbubbles, anti-PD-L1 antibody, miR-34a, cervical cancer

Introduction

According to statistics, cervical cancer is considered to be the fourth most common and lethal gynecological malignant tumor in females [1], but traditional cancer treatment, such as surgery, chemotherapy and radiotherapy, is often ineffective because of genetic heterogeneity and multi factor characteristics of drug resistance. Recently, cancer immunotherapy has shifted the paradigm for the treatment of cancer [2]; the purpose of immunotherapy is to activate or enhance the activation of anti-tumor immune system, provide exogenous immunogenic stimulation, and antagonize the regulatory pathway of inducing immune tolerance [3].

Immunotherapy is considered to be a more effective option to cancer therapy [4].

At the same time, gene therapy which works by transfecting exogenous genes to promote apoptosis of tumor cells is also considered to be a promising treatment for cancer. The key of gene therapy is to deliver specific gene to the target area effectively with appropriate carriers [5]. Among investigated agents, ultrasound targeted microbubble destruction (UTMD) can be an efficiently and specifically to deliver targeted microbubbles (MBs) to tumor tissue combined with ultrasound [6]. This delivery system not only increases the permeability of endothelial cells and tissues, but also allows microbubbles

to specific sites, and promotes the entry of genes or drugs into cells, thus significantly improving the therapeutic effect [7].

Purpose of present research is to explore synergistic inhibitory effect of ultrasound-mediated anti PD-L1 antibody and miR-34a MBs, and try to provide a new treatment for cervical cancer.

Materials and methods

Preparation of targeted microbubbles

The preparation of cationic microbubbles used the method of thin-film hydration. Microbubble shell was consisted of 1,2-distearoyl-sn-glycero-3-phosphatidylcholine (DSPC, Avanti Polar Lipids, INC, USA), 1,2-distearoyl-sn-glycero-3-phosphoethanolamine-N-[methoxy (polyethylene glycol)-2000] (DSPE-PEG-2000, Avanti Polar Lipids, INC, USA). Branched-chain poly-etherimide-600 (PEI-600, Avanti Polar Lipids, INC, USA). PEI can provide a positively charged surface for the microbubbles, which prepared for conjugating gene. These materials were dissolved in a chloroform with a molar ratio of 9:5:5. The thin lipid film was formed with water bath at 55°C and inflated with a steady stream of nitrogen, meanwhile, the residual chloroform was removed by vacuuming for 3 hours. Then the lipid film was dissolved by Tris buffer which compose of 10:10:80 (v/v/v) 0.1 M Tris-buffered saline: glycerol solution: propylene glycol (pH 7.4). Then put bottle in a 60-70 degree ultrasonic cleaner to make sure the film was fully dissolved, finally it was sub-packaged, sealed, vacuumed and filled with Octafluoropropane (C_3F_8, Wuhan Newradar Special Gas Co., Ltd., Wuhan, China) gas replacement.

In order to preparation the biotinylated microbubbles, 1,2-distearoyl-sn-glycero-3-phosphoethanolamine-N-[biotinyl (polyrthylene glycol)-2000] (DSPE-PEG-2000-Biotin, Avanti Polar Lipids, INC, USA) can replace the DSPE-PEG-2000. When the biotinylated microbubbles were prepared, 3 µl streptavidin (Beijing Bioss Biotechnology Co., Ltd.) was added to 100 µl microbubbles for 30 min at room temperature. And biotinylated monoclonal PD-L1 antibody was mixed with the streptavidin/biotinylated microbubbles in a 4:100 volume ratio for 4 h at 4°C. PD-L1 Ab-MBs was washed by phosphate-buffered saline (PBS) to remove the unbound

antibody. When targeted PD-L1 Ab-MBs were prepared, then contact miR-34a (1000 µg/mL) by electrostatic adsorption in a 2:100 volume ratio, for 30 min at room temperature, so the PD-L1 Ab/miR-34a MBs were equipped.

To confirm PD-L1 antibody was conjugated to the biotinylated microbubbles, 10 µl P-phycoerythrin-labeled streptavidin (streptavidin/PE, Beijing Bioss Biotechnology Co., Ltd.) was added to 200 µl biotinylated microbubbles and mixed at room temperature for 30 min, then cleared the free PE-conjugated streptavidin by low speed centrifugation and the upper liquor was washed by PBS. Excess biotinylated PD-L1 antibody (Anti-Mouse B7-H1-biotin, eBioscience, San Diego, California, USA) were added to adhered to biotinylated lipid microbubbles. 1 µl fluorescein isothiocyanate-labeled (FITC) secondary antibody (Santa Cruz Biotechnology Co., Ltd., USA) was added to 50 µl microbubbles and mixed for at least eight hours (or overnight). The free FITC-labeled secondary antibody were removed by low speed centrifugation and PBS washed. By detecting the bright red and green fluorescence on the surface of microbubbles to conform the conjugation of anti-PD-L1 antibody.

To analyze the characteristics of the anti-PD-L1 antibody conjugated microbubbles, non-biotinylated lipid microbubbles as a control. The biotinylated microbubbles was observed by Optical microscope, the anti-PD-L1 antibody conjugated microbubbles were examined using Confocal microscope and the zeta and size were measured by Zeta Sizer analyzer instrument (Zeta Sizer, Sichuan, China).

Cell culture

U14 cervical cancer cell lines were obtained and stored st the Three Gorges University Tumor microenvironment and Immune Therapy Laboratory, and the U14 cell were cultured in Dulbecco's modified Eagle's medium (DMEM) in humidified environment of 5% CO_2, 37°C.

Targeting assay

This experiment aims to detect the capacity of anti-PD-L1 antibody microbubbles targeted to U14 cells. U14 cells were planted in 6/12/24-well plate in a humidified atmosphere for 24 hours to allow cell adhesion. After that, the

anti-PD-L1 antibody conjugated microbubbles ($1×10^5$/ml) and the non-conjugated microbubbles ($1×10^5$/ml) were added to the petri plate respectively. After a 30 minute mixed, remove the unbound microbubbles through washed the cells by PBS for three time.

Contrast-enhanced ultrasound imaging (CEUS)

The planted tumor was established in the right anterior axillary region of mouse, and when the mean diameter of tumors up to 5 mm allowed to CEUS. Mice were narcotized in inhaling 2% isoflurane at the rate of 1.2 L/min, and using electric blanket to keep them warm during the whole operation. Contrast-enhanced ultrasound imaging were operated by Mindray RE-7 (Mindray Medical International Co., Ltd. China), which equipped with 18 MHz central frequency linear probe. Then, 200 μl of MBs, PD-L1 Ab-MBs or PD-L1 Ab/miR-34a-MBs were injected intravenously via the tail vein (per injection of $1×10^8$ MBs in 200 μl) (n = 3) to evaluate the capability of contrast imaging in vivo. And quantitative analyses by Sonamath software (AmbitionT. C., China).

Transfected gene expression

1 ml U14 cells suspension that set 4 duplicate holes were added into 24-well plates and added 50 μl cationic microbubbles which loading pEGFP plasmid. The ultrasound was setting at different irradiation power and irradiation times. After 24 hours of irradiation, the expression of pEGFP plasmid was detected by fluorescence microscope.

Animal experiment

Fifty specific pathogen free (SPF)-level female BALB/c mice, about 5-6-week-old, weighing-25 g, were provided and maintained by the Animal Experimental Center of the Three Gorges University. Subcutaneous mouse cervical cancer xenograft tumors were established in the right front armpit region by subcutaneous injected U14 cells with a density of 10^6/200 μL cells. The planted tumor was allowed to experiment when the mean diameter of tumors up to 5 mm (range, 3-8 mm).

Fifty mice were successfully modeled randomly to divide into control group, empty microbubbles and ultrasound group (MBs + US), targeting PD-L1 Ab microbubbles + ultrasound group (PD-L1 Ab-MBs + US), miR-34a lorded microbubbles (miR-34a-MBs + US), targeting PD-L1 Ab combined with miR-34a microbubbles + ultrasound group (PD-L1 Ab/miR-34a-MBs + US), ten mice in each group. All the microbubbles were injected intravenously via the tail vein (per injection of $1×10^8$ MBs in 200 μL) n = 10. Along with each injection, the planted tumor should be irradiate immediately by ultrasound. Ultrasound parameters were set at 1 W/cm^2 for 90 s, with duty circle of 50%. The above treatment once every two days, and the size of the implanted tumor was measured at 1, 3, 5, 7, 9 days with a ruler. Tumor volume was calculated by Volume = length (width)^2/2. Tumor growth inhibition (TGI) was calculated by TGI (%) = (1-Tumor weight or volume of treated group/Tumor weight or volume of control group) ×100%. After 5 times of the ultrasound-targeted microbubble destruction treatment, deprived the planted tumor and spleen from mice.

Hematoxylin eosin stain

Hematoxylin eosin staining (H&E) was used to evaluate the degeneration, necrosis, and inflammation. After fixation with formalin, paraffin embedding was performed, and serial sections were prepared for H&E staining. The slide was observed by microscope.

Tunel assay

The paraffin section was carried out by the instructions of TUNEL apoptosis detection kit. The appearance of red fluorescently labeled apoptotic bodies in the nucleus of tumor cells were regarded as positive reaction. The apoptotic staining was observed by laser confocal microscopy. Apoptosis index (AI) = apoptotic cells/total cells ×100%.

Immunohistochemistry

The tumor tissue was fixed with 4% paraformaldehyde, dehydrated, embedded in paraffin, and with a graded alcohol sliced. After standard dewaxing, rehydration and antigen repair, endogenous peroxidase was blocked by 3% H_2O_2. Primary antibodies against Bcl-2 (1:200) and Bax (1:200) was added to sections and incubated at 4°C for overnight. After rewarming, the slides were added into goat anti-mouse secondary antibody and incubated for an hour

at room temperature. DAB reagent (Boster Biological Technology co. ltd in Wuhan, China) dripped on the sections for 30 minutes, then, washed and naturally dried. The cut surface was covered with neutral resin, finally the sections were observed by microscope.

RT-PCR

Trizol reagent (TaKaRa) was used to extract the total RNA of tumor tissue, and using the PrimeScriptTM RT Kit (TaKaRa) to reverse RNA transcripte into cDNA, then each cDNA sample was analyzed by Applied Biosystems. The Real-Time PCR System was operated by manufacturer's protocol of SYBR Premix Ex Taq II (TaKaRa). The relative mRNA expression of Bcl-2, Bax, TNF-α, and INF-γ was calculated by cycle threshold (Ct) method.

Immunofluorescence

The section for immunofluorescent was prepared. Immunofluorescent was performed on 4-μm-thick tumor slices. The following primary antibodies were used: PE-conjugated anti-PD-L1 Ab (1:1000) and isothiocyanate (FITC)-conjugated anti-CD8 (1:100) monoclonal antibody. Cell nuclei were counterstained with DAPI. Confocal microscope was used to detect the immune response region at 600× magnification fields.

Flow cytometry

The spleen of the mice was cut into pieces and dissociated into RPMI 1640 medium. Splenic cells were suspended in 2 ml 0.1% PBS and 1.2 μl Carboxyfluorescein Diacetate Succinimidyl Ester (CFDA-SE). Then, the cell concentration was adjusted to 10^6/ml. Splenic cells were inoculated into 24-well plate. The group was different from the culture medium with tumor antigen or without tumor antigen. The plate was incubated at 5% CO_2, 37°C for 48 h. Then, IL-2 were added to 24-well plate at the same condition for 48 h. After 96 h, spleen cells were collected by centrifugation at speed of 1500 rpm/min for 3 min and washed by PBS three times, then lymphocyte proliferation was analyzed by flow cytometer.

Lactate dehydrogenase leakage assays

The spleen cells were co-cultured with U14 cells for 3 h, and the lactate dehydrogenase detection solution was prepared according to the instructions of the lactate dehydrogenase kit. 60 μl lactate dehydrogenase detection solution was added to each sample, and incubated for 20 min at room temperature. Then detected the absorbance (OD) at 490 nm with the enzyme micrometer. Finally, calculated the cell killing rate following the formula: KR (killing rate) = $(OD_k-OD_b) (OD_m-OD_b)^{-1} \times 100\%$ (OD_k: OD value of killing effect group, OD_b: OD value of blank group, OD_m: OD value of maximum release group).

Statistical analysis

One-way ANOVA followed by the student Newman-Keuls post hoc test (t-test) and Least significant difference (LSD) were used to test the differences of expression among the five groups. Chi-square test was applied to estimate the differences on qualitative data. Quantitative date are presented as mean ± SD. A p-value <0.05, p-value <0.01 indicated statistically or extremely significant. Qualitative data are shown as number (%). Statistics were analyzed by SPSS 18.0 (SPSS Inc., Chicago, USA).
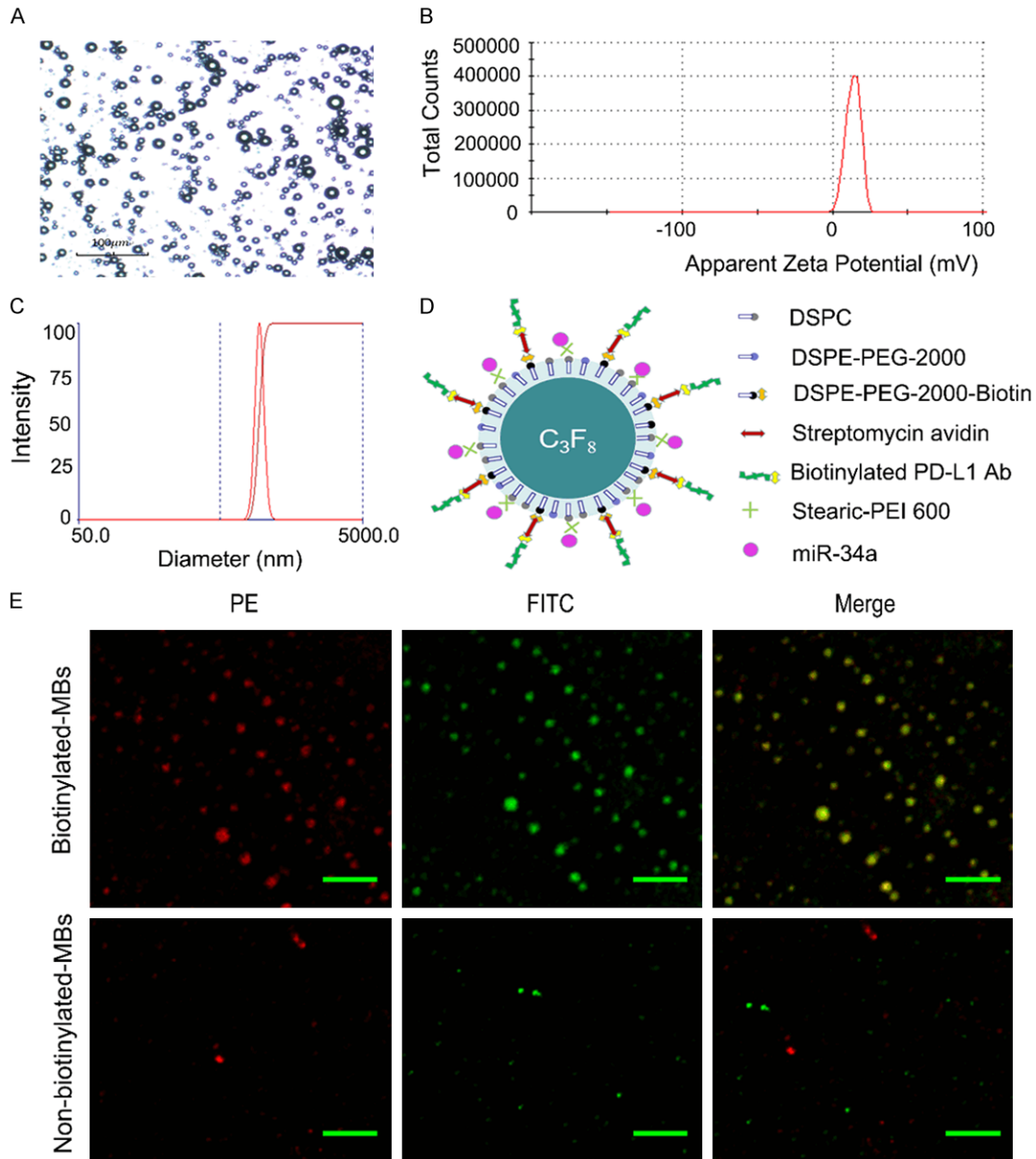
Result

Preparation and characterization of PD-L1 Ab/ miR-34a-MBs

The cationic microbubbles were observed by optical microscope, the microbubbles were round with regular characters and uniform particle size distribution, no agglomeration, which conformed to the experimental requirements (**Figure 1A**). The cationic microbubbles had a size distribution of 938.9±80.0 nm and the apparent zeta potential was 17.7±3.8 mV (**Figure 1B**, **1C**). The microbubbles' mean concentration was 4.6×10^7 MBs/mL which measured by blood cell count plate.

Biotinylated microbubbles were prepared by first complexing the avidin to cationic microbubbles, then attached to the biotinylated PD-L1 antibody (**Figure 1D**). To demonstrate effective loading, we performed confocal microscopy on microbubbles that were combined with FITC conjugated anti-mouse IgG to bind to PD-L1 antibody loaded on microbubbles (excited at 488 nm, emitted at 530 nm). The combination of biotinylated microbubbles with PE-avidin was

Figure 1. Identification of the prepared targeted microbubbles. A. Characterization of cationic microbubbles were observed by optical microscope (×400); B. The apparent zeta potential of cationic microbubbles was 17.7±3.8 mV. C. The cationic microbubbles had a size distribution of 938.9±80 nm; D. PD-L1 Ab/miR-34a MBs structure diagram; E. Observed PD-L1-Ab conjugation to biotinylated microbubbles and non-biotinylated microbubbles by laser confocal microscopy (PE: streptavidin-PE; FITC: rabbit anti-mouse IgG-Fc/FITC) (×400), scale bar = 50 µm. Red fluorescence indicates that streptavidin-PE binds to the biotin of the microbubble, and green fluorescence indicates that the FITC-labeled secondary antibody binds to the mouse anti-PD-L1 antibody and then links with the microbubbles.

verified by detected the red fluorescent around the microbubbles surface. While, the combination of the secondary antibody with avidin-biotinylated microbubbles was verified by detected the green fluorescent around the microbubbles surface. Confocal images showed colocalization of PD-L1 antibody with the biotinylated microbubbles by means of biotin-strepavdin conjugation. The images were all acquired at 600× magnification, avdin was visualized with

580 nm (red), secondary antibody was visualized with 488 nm (green) (**Figure 1E**).

Examined the targeting and contrast-enhanced efficiency of targeted-MBs

The expression of PD-L1 on U14 cytomembrane was detected by laser confocal microscopy. High expression of red fluorescence was observed by laser confocal microscopy indicated that PE labeled PD-L1 antibody conjugated to the U14 cytomembrane (**Figure 2A**). The experiment examined the targeting efficiency of non-targeted MBs and targeted MBs to U14 cells. For non-targeted MBs, only a slight non-specific binding to U14s was observed; however, more targeted MBs bound to U14 were observed. As observed under the light microscope (**Figure 2B**), the results were presented that, the combination rate in non-targeted MBs and targeted MBs were significant different, which indicated that targeted MBs has a higher targeting ability to U14 cells.

All of the MBs, PD-L1 Ab-MBs and PD-L1 Ab/miR-34a-MBs had well contrast imaging capabilities in vivo (**Figure 2C**). The peak intensity and the time to peak showed no significant difference among the groups (**Figure 2D**, **2E**).

Quantitative assessment of ultrasound-targeted microbubble destruction (UTMD)-mediated gene transfection in U14 cell

Firstly, we conformed that 25 μl MBs has the capacity of loading 1 μg plasmids (**Figure 3A**). To detect the ultrasound-mediated destruction increasing EGFP gene expression in U14 cell, semi-quantitiative PCR analyses the delivery of EGFP plasmid to U14 cells 48 hours following UTMD-mediated gene transfection. The results indicated that under the power was 1 W/cm^2 and the time was 25 second, the expression of EGFP mRNA was significantly increased (**Figure 3B**).

UTMD mediated delivery of EGFP gene was tested in the U14 cells. The EGFP plasmid was used for fluorescence imaging of gene transfection efficiency. The fluorescence microscopic images showed that EGFP-MBs + US group exhibited the highest fluorescence emission, the results indicated that UTMD-mediated could improve the gene transfection efficiency (**Figure 3C**).

Tumor growth inhibition

Schematic illustration showing the treatment process just like the **Figure 4A**. The implanted tumor was measured every two days at 1, 3, 5, 7 and 9 days and the tumor volume was calculated (**Figure 4B**). The gross tumor volume was increased in all groups, especially in control group and MB + US group, tumor tissue was removed after the treatment and the tumor inhibition rate was calculated (**Figure 4C**). The results showed that the volume inhibition rates of PD-L1 Ab-MBs + US, miR-34a-MBs + US and PD-L1 Ab/miR-34a-MBs + US were 35.38%, 40.50% and 54.32%, and the mass inhibition rates were 35.80%, 42.43% and 60.14% (**Table 1**). Compared to control group, the weight and volume of tumor became less in all the three treatment groups (P<0.05). Among them, the inhibitory effect of PD-L1 Ab/miR-34a-MBs + US group was more obvious (P<0.01). The tumor volume and weight inhibition rate in different groups were shown in **Table 1**. The data showed that PD-L1 Ab/miR-34a-MBs + US delivery system showed a potential inhibitory effect, PD-L1 antibody combine miR-34a could synergistic inhibit cervical cancer cells synergistic.

Tumor tissue damage revealed in histological observation

H&E staining was used to reveal the anti-tumor effects of targeted MBs treatment. The results showed that the arrangement of tumor cells was disordered, meanwhile, tumor cells were active in growth and nucleic division was obvious, and tumor cells with large nuclear-cytoplasmic ratios and significant profile in the control group and MBs + US group. By contrast, there are extensive necrosis of tumor tissue in targeted-MBs group, but little in the control group and MBs + US group, the most obvious necrosis was observed in the PD-L1 Ab/miR-34a-MBs + US group (**Figure 5A**).

*Mechanism of targeted microbubbles inducing apoptosis*

Effects of targeted microbubbles treatment on the apoptotic induction of tumor cells: TUNEL was widely used to quantitative evaluation of apoptosis. The cells with bright red-stained nuclei were apoptotic cells, AI can be calculated. Positive apoptotic cells in PD-L1 Ab-MBs + US group and miR-34a-MBs + US group were
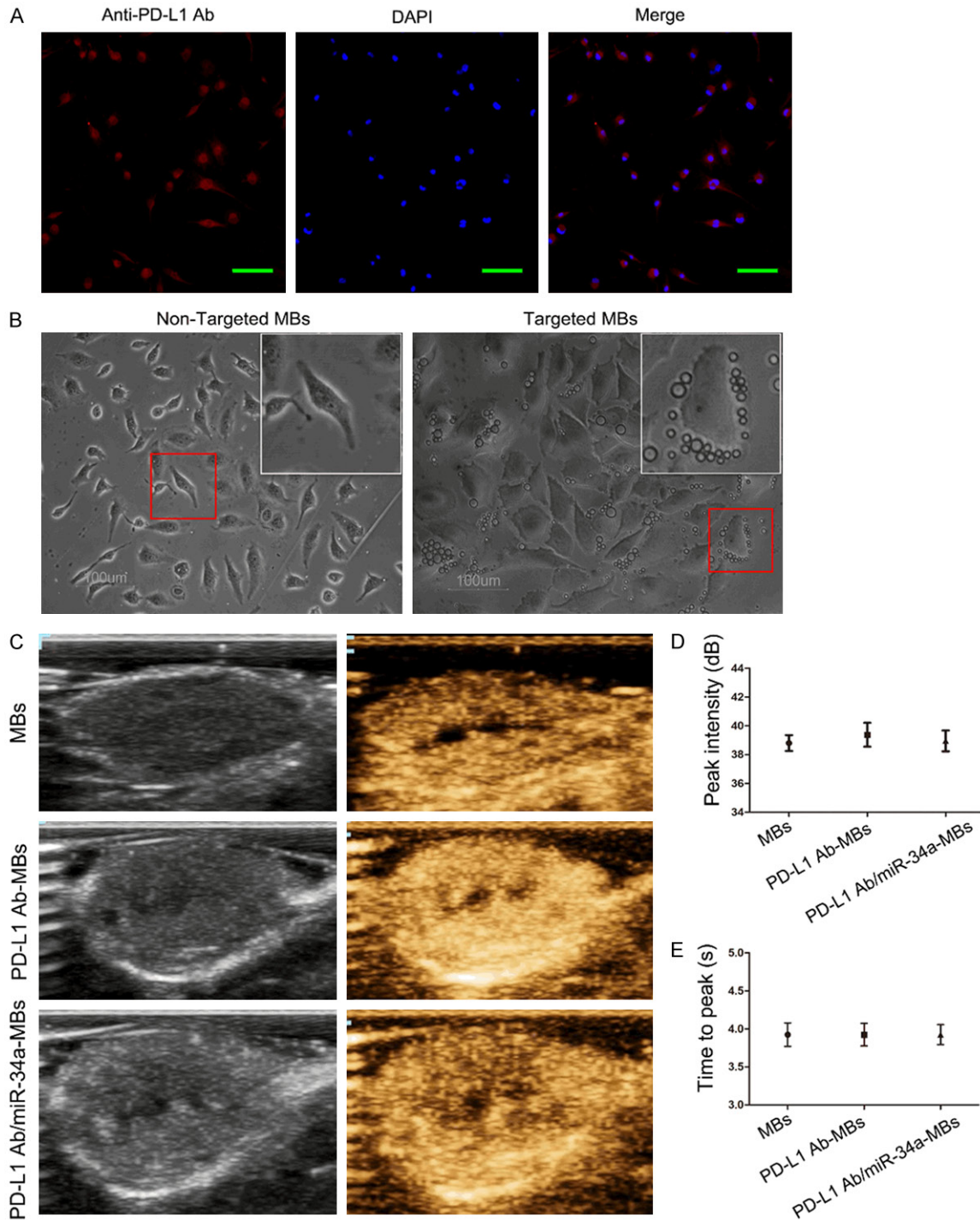
Figure 2. Examined the targeting and contrast-enhanced efficiency of targeted-MBs in intro and vivo. (A) PD-L1 expression on U14 membranes was confirmed by laser confocal microscopy. High expression of red fluorescence was observed on the U14 membranes (×200), scale bar = 100 μm; (B) Non-targeted microbubbles (NMBs) and targeted microbubbles (TMBs) were observed bind to U14 cells by light microscope (×400), with NMBs, only a slight non-specificity binding to U14s was observed; comparatively, it can be observed that the U14 cells were surrounded by TMBs; (C) The results of Contrast-enhanced Ultrasound Imaging showed that all of the MBs, PD-L1 Ab-MBs and PD-L1 Ab/miR-34a-MBs had well contrast imaging capabilities in vivo. The peak intensity (D) and the time to peak (E) of Contrast-enhanced Ultrasound Imaging in vivo have no significant difference among the groups (*P>0.05*). Date in figure D&E are presented as mean ± SD, n = 3.
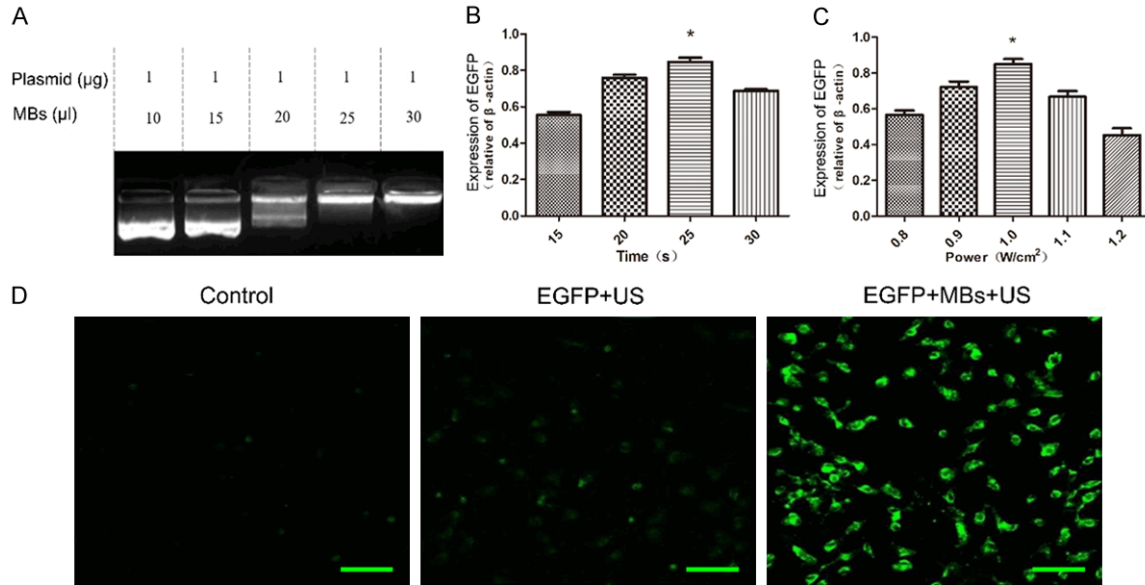
Figure 3. The UTMD promoted gene transfection into U14 cells through the DNA loaded targeted microbubbles. A. Analysis of DNA loading capacity of the MBs. The result of agarose gel electrophoresis (AGE) showed that the 25 µl MBs has the capacity of loading 1 µg plasmids. B, C. Quantitative assessment of UTMD-mediated gene transfection in U14 cell with different irradiation power and time; D. The fluorescence microscopic images showed that, control group and EGFP pasmid + US group exhibit negligible fluorescence emission, while, EGFP plasmid-MBs + US group exhibited the higher fluorescence emission (×200), scale bar = 100 µm.
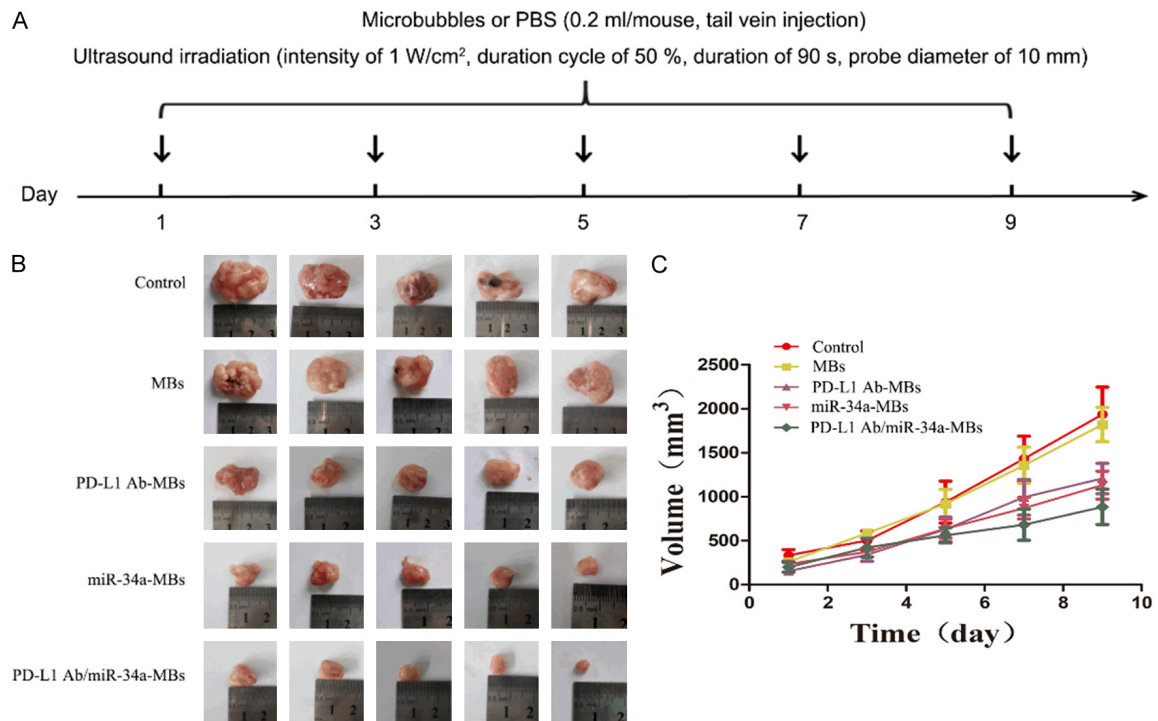
Figure 4. The in vivo therapeutic effects of the targeted microbubbles in the U14 cervical carcinoma bearing mice. A. Schematic illustration of the therapeutic formulations. Mice were injected with different types of microbubbles, while in control group were injected with equal dosage of PBS, and each group was irradiated by ultrasound with specific parameters every two days (n = 10). B. Representative tumor tissues excised from the mice at the end of the treatment; C. Tumor volume growth curve. The tumor volume of the control group and MBs + US group showed an exponential growth pattern, and the tumor growth of the other groups was slowed down.

Table 1. Comparison tumor growth inhibition in different groups

Group	tumor volume (mm^3)	Volume inhibition rate (%)	tumor weight (g)	Weight inhibition rate (%)
A	1933.83±694.16	0	2.71±1.55	0
B	1829.31±436.29	5.38	2.63±0.68	2.95
C	1249.24±448.84	35.38*	1.74±0.91	35.80*
D	1150.11±406.12	40.50*	1.56±0.57	42.43*
E	883.11±447.73	54.32**,#	1.08±0.28	60.14**,#

A: Control group; B: microbubbles + ultrasound group (MBs + US); C: anti-PD-L1 antibody MBs + ultrasound group (PD-L1 Ab-MBs + US); D: plasmid pcDNA3.1 (+)-miR-34a MBs + ultrasound group (miR-34a-MBs + US); E: PD-L1 Ab/miR-34a MBs + ultrasound group (PD-L1 Ab/miR-34a-MBs + US). Chi-square test was used to estimate the differences on this qualitative data. Compared with the control group, *P<0.05, **P<0.01; Compared with other groups #P<0.05. n = 10.

increased significant (P<0.05). Meanwhile, the positive staining had a remarkable increasing in PD-L1 Ab/miR-34a + US group compared to control group (P<0.01) (**Figure 5B**). The cells with red-stained nuclei was showed in all the groups (**Figure 5C**). The result revealed that PD-L1 antibody and miR-34a could promote tumor cell apoptosis, what's more, immunotherapy with PD-L1 Ab in combination with miR-34a is able to synergistically improve the efficacy to promote tumor cell apoptosis.

Effects of targeted microbubbles treatment on the induction of apoptotic related gene

Expression: Bcl-2 and Bax are an important related genes of apoptosis. The expression products of Bcl-2 and Bax exist inside the same cell in the form of homodimers or heterodimers. When there is over-expression of Bax and forms homodimers Bax/Bax it promotes apoptosis and when there is over expression of Bcl-2 to form heterodimers Bcl-2/Bax it promotes cell cycle and cell proliferation and inhibition of apoptosis [8]. We not only detected the expression of Bcl-2 and Bax protein in tumor tissue by immunohistochemical staining (**Figure 6A**, **6B**), but also examined the levels of Bcl-2 and Bax mRNA by RT-PCR (**Figure 6C**). These findings demonstrate that the level of Bcl-2 downregulated while the level of Bax upregulated with the treatment of targeted-MBs. The changes of Bcl-2 and Bax mRNA expression in treatment groups showed the same trends.

MiR-34a down-regulation had closely related to differentiation and metastasis in cervical cancer [9], the research indicated that the expression of miR-34a in PD-L1 Ab-MBs + US group and PD-L1 Ab/miR-34a-MBs + US group were up-regulated, compared to control group (P<0.05), the up-regulated was more significant in PD-L1 Ab/miR-34a-MBs + US group (P< 0.01) (**Figure 6D**).

Mechanism of targeted microbubbles inducing antitumor immunoresponse

*Effects of targeted microbubble treatment on the expression of PD-L1 and CD8+:* Immunofluorescence results revealed the expression of PD-L1 protein in tumor cell in PD-L1 Ab + US group and PD-L1 Ab/miR-34a + US group were downregulated remarkably as compared with control group using PE-conjugated anti-PD-L1 monoclonal antibody staining, indicating that PD-L1 antibody-MB could block the PD-L1 molecule on the high expression of cervical cancer cells, and relieve local inhibitory tumor immuno-microenvironment (**Figure 7A**).

CD8+ T cells played a key role in immune system. The expression of CD8+ T cells were observed using isothiocyanate (FITC)-conjugated anti-CD8 antibody staining, and upregulated in PD-L1 Ab + US group, miR-34a + US group and PD-L1 Ab/miR-34a + US group as compared with control group (**Figure 7B**). The result indicated that PD-L1 antibody and miR-34a can promote cytotoxic T-cells proliferation, enhancing the killing effect of T-cells.

Effects of targeted microbubble treatment on the expression of cytokine: To assess the expression of cytokines associated with antitumor immunity induced by anti-PD-L1 antibody alone or in combination with miR-34a gene, we examined the level of TNF-α and INF-γ mRNA in tumor tissue by RT-PCR. The results revealed that with the treatment of PD-L1 Ab-MBs or miR-34a MBs caused a significant increasing in the level of TNF-α and INF-γ compared to control group (P<0.05). Moreover, the expression of TNF-α and INF-γ were markedly upregulated in combination therapy group (PD-L1 Ab/miR-34a-MBs + US) (P<0.01; **Figure 7C**, **7D**).

Enhanced spleen lymphocyte proliferative responses following targeted microbubbles treatment: CFSE labelling has been widely used to reveal and track cell proliferation. Flow cytometry detected the proliferation of Spleen
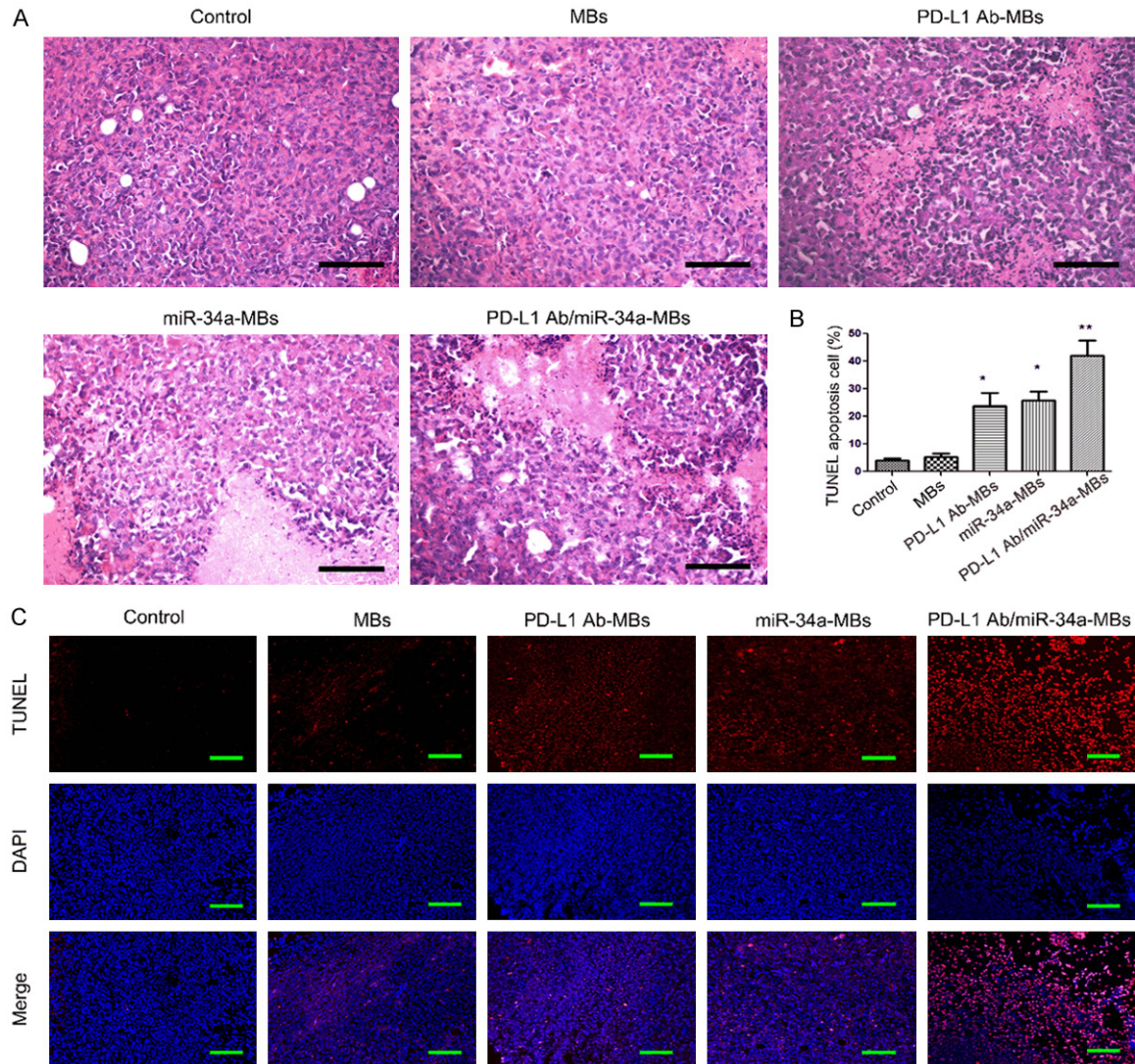
Figure 5. Analysis of the apoptosis of tumor tissues after the treatment. (A) Histopathology of tumor tissues in each group (H&E, ×400), scale bar = 200 μm. The histological sections were prepared from various tumor tissues in the mice. In the control group or MBs + US group the tumor histopathological sections showed that the arrangement of tumor cells was disordered, tumor cells active growth and evident nucleic division, and tumor cells with large nuclear-cytoplasmic ratios and significant profile; While in the targeted MBs the tumor histopathological sections revealed that the tumor cells extensive necrosis, especially in the PD-L1 Ab/miR-34a-MBs + US group; (B) The semi-quantification analysis of apoptotic cells in tumor tissues of each group by the fluorescence intensity showed in (C) (Compared with the Control group, $*P<0.05$, $**P<0.01$). (C) TUNEL assay was used to analyse cell apoptosis. Red-stained nuclei indicate cells in the apoptotic state (original magnification, ×200), scale bar = 100 μm.

lymphocyte labeling with CFSE, proliferation index (evaluated lymphocyte proliferative responses) represent for activity of lymphocyte proliferation. After 96 h with or without tumor antigen stimulation in vitro, spleen lymphocyte were detected by flow cytometry. The result displayed that, with or without tumor antigen stimulation, there is no obvious effect on lymphocytes proliferation in control group and MBs + US group, expecting for a small amount of self-

proliferation (**Figure 8A**). Whereas, with tumor antigen stimulation, significant difference were observed in PD-L1 Ab-MBs + US group, miR-34a-MBs + US group and PD-L1 Ab/miR-34a-MBs + US group, proliferation index increased significant compared to control group (P<0.05) (**Figure 8B**). Without stimulation, there is no significant difference between all the groups (**Figure 8C**). The result indicated that lymphocyte proliferative responses were active and
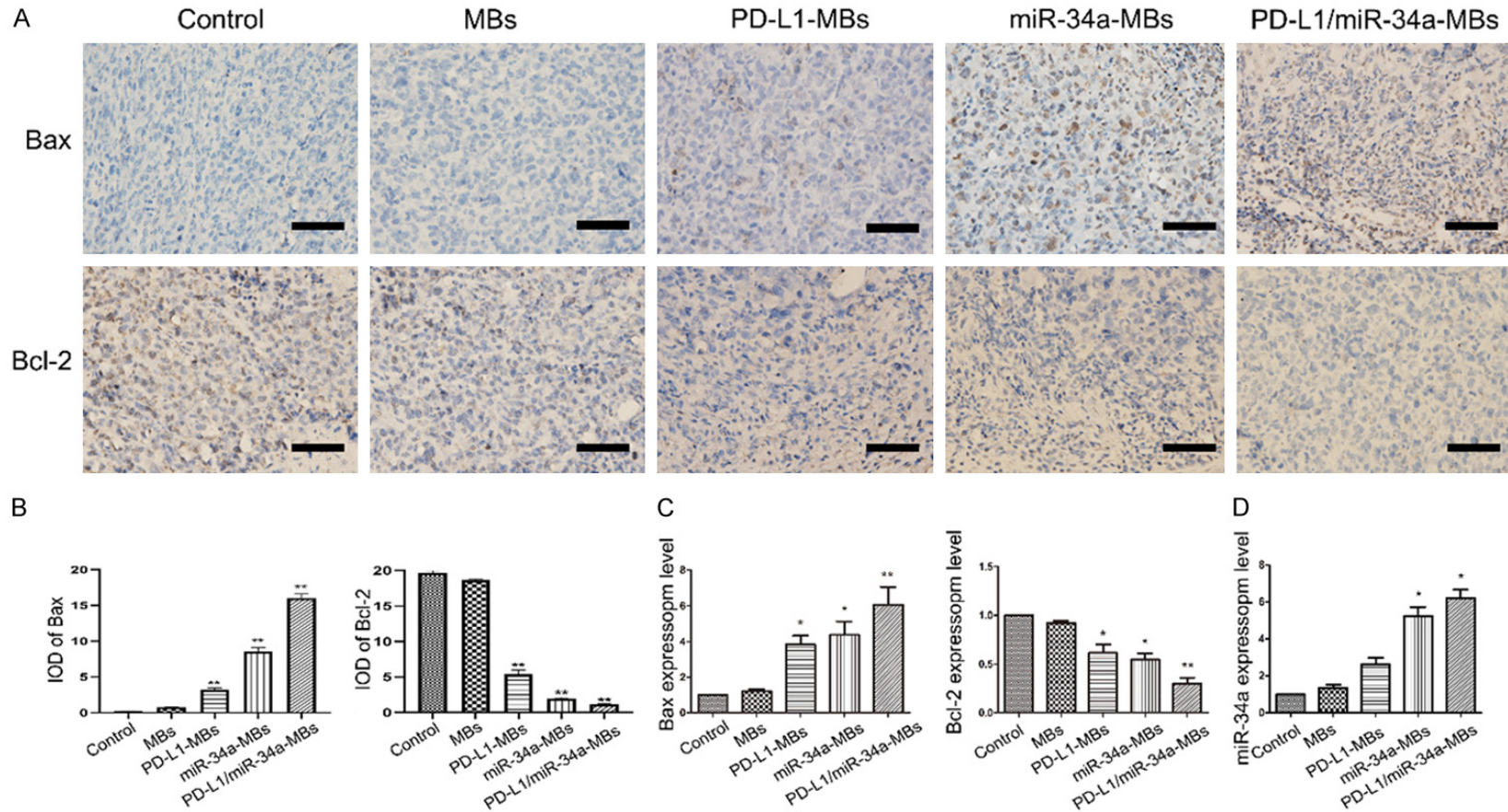
Figure 6. Expression of Bcl-2 and Bax in the tumor tissues. (A) Detection of Bax and Bcl-2 protein expression in tumor tissues by immunohistochemistry staining (×400), scale bar = 200 μm. (B) Data were processed using ImageJ software. The protein expression of Bax shown in (A) was significantly higher in the PD-L1 Ab-MBs + US group, miR-34a-MBs + US group and PD-L1 Ab/miR-34a-MBs + US group, while the results of Bcl-2 expression were reversed. (C) The mRNA expression of Bax and Bcl-2. The expression of Bax gene in all the treatment groups was higher than that in the control groups, the PD-L1 Ab/miR-34a-MBs + US group was most obvious. While the results of Bcl-2 were reversed. (D) The mRNA expression of miR-34a. The expression of miR-34a gene were up-regulated in the treatment groups, especially in the miR-34a-MBs + US group and PD-L1 Ab/miR-34a-MBs + US group. (Compared with the control group, *$P<0.05$; **$P<0.01$, n = 10).
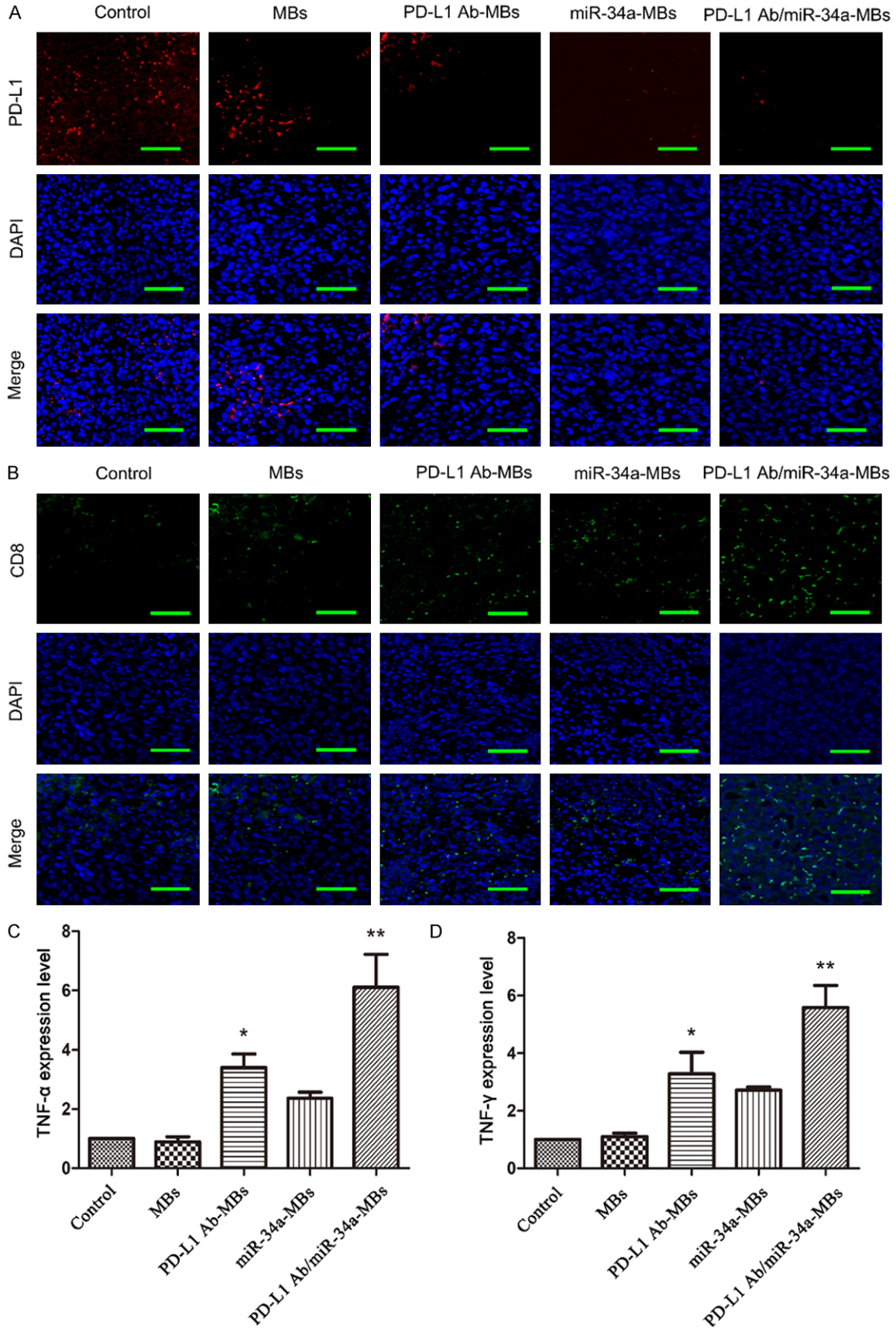
Figure 7. The anti-tumor immunotherapy with the targeted microbubbles. A. Expression of PD-L1 in each group detected by immunofluorescence (original magnification, ×600), scale bar = 50 μm. The expression of PD-L1 was significantly downregulated in the PD-L1 Ab/miR-34a-MBs + US group compared to Control group. B. Expression of CD8-positive T cells in each group detected by immunofluorescence (original magnification, ×600), scale bar = 50 μm. In addition to the Control group, the number of CD8 T cells in each group of tumor tissues increased, and green fluorescence was emitted significant in PD-L1 Ab/miR-34a-MBs + US group under laser confocal microscope. C, D. The mRNA expression of IFN-γ and TNF-α. The expression of IFN-γ and TNF-α gene in all the treatment groups was higher than that in the control groups, the increased in PD-L1 Ab/miR-34a-MBs + US group was most obvious. (Compared with the Control group, *$P<0.05$; **$P<0.01$, n = 10).

immune activity were enhanced with the treatment of targeted MBs.

Effects of targeted microbubbles treatment on the cytotoxicity of lymphocytes

Lactate dehydrogenase is an important enzyme in the cytoplasm. When cells are attacked by factors, lactate dehydrogenase will be released. The cytotoxic killing effect can be reflected by LDH assays. The results showed that, the cytotoxic cell killing rate increased significant in PD-L1 Ab-MBs + US group and miR-34a-MBs + US group ($P<0.05$), among all the groups the increasing of cytotoxic cell killing rate was more significant in PD-L1 Ab/miR-34a-MBs + US group ($P<0.01$). It may indicate that both PD-L1 antibody and miR-34a had capacity to enhance the cytotoxic effects of lymphocytes to regulate the immune. PD-L1 antibody and miR-34a may has the effect of coordination enhancement on anti-tumor therapy (**Figure 8D**).

Discussion

Targeted cancer therapy was considered to be a promising treatment for its utilizing surface receptors that are highly expressed on tumor cells [10]. Ultrasound-mediated microbubble destruction (UMMD) has exerted enormous potential in targeted cancer therapy for the past few years, and it can induce the destruction of cytomembrane and enhance the permeability of cytomembrane by acoustic cavitation and inducing the production of physical forces, such as shock wave, implosion, microflow and liquid jet [11]. Therefore, molecules such as antigens or genes encoding antigens loaded in the microbubbles can be delivered into the tumor tissue specifically and efficiently with combination of ultrasound [12], in addition, antibodies, genes, drugs, and cytokines can be delivered into the cytoplasm of immune cells directly [13]. Particularly, it has been proved

that UMMD has better gene delivery efficiency than viral vectors [14]. Pysz developed an VEGFR-2-targeted microbubble destruction delivery system which had a good targeting property in the mouse pancreatic cancer model and had inhibitory effect on tumor cells [15], and the miR-34a gene carrying microbubbles can promote the apoptosis of multiple myeloma cells [16]. Microbubbles served as a vehicle, it can carry more than one drug or gene, and systemic co-administration was considered to be more effective. Recently, it has been proved that co-delivery of miR-34a and PTX, achieved a synergistic effects to enhance anticancer capacity in cervical cancer [17]. In this study, we developed three kinds of targeted-microbubbles: PD-L1 Ab-MBs, miR-34a-MBs, PD-L1 Ab/miR-34a MBs, and to verify which targeted microbubbles works best. From the results obtained in the study, PD-L1 Ab/miR-34a-MBs were successfully constructed, it had good targeting and automatic target seeking ability. What's more, the addition of PD-L1 antibody to MBs did not affect miR-34a loading capacity significantly. PD-L1 Ab/miR-34a-MBs showed an excellent capability to target U14 cells in vitro and had well contrast imaging capabilities in vivo. The main mechanism for its targeting is the reaction between the antigen and antibody, so the targeting capacity makes no difference after loading miR-34a. The excellent advantages associated with using anti-PD-L1 antibody targeted MBs to enhance ultrasound-mediated miR-34a transfer in vivo and vitro and multiple targeted microbubbles strengthened the inhibition of tumor growth effect.

Immunotherapy, which has a unique advantage of high specificity characteristically for the tumor cell without influencing normal cells, holds vast prospect for cancer treatment [18]. The combination of US and microbubbles play a key role in delivering immunostimulatory substances to response the antitumor immune
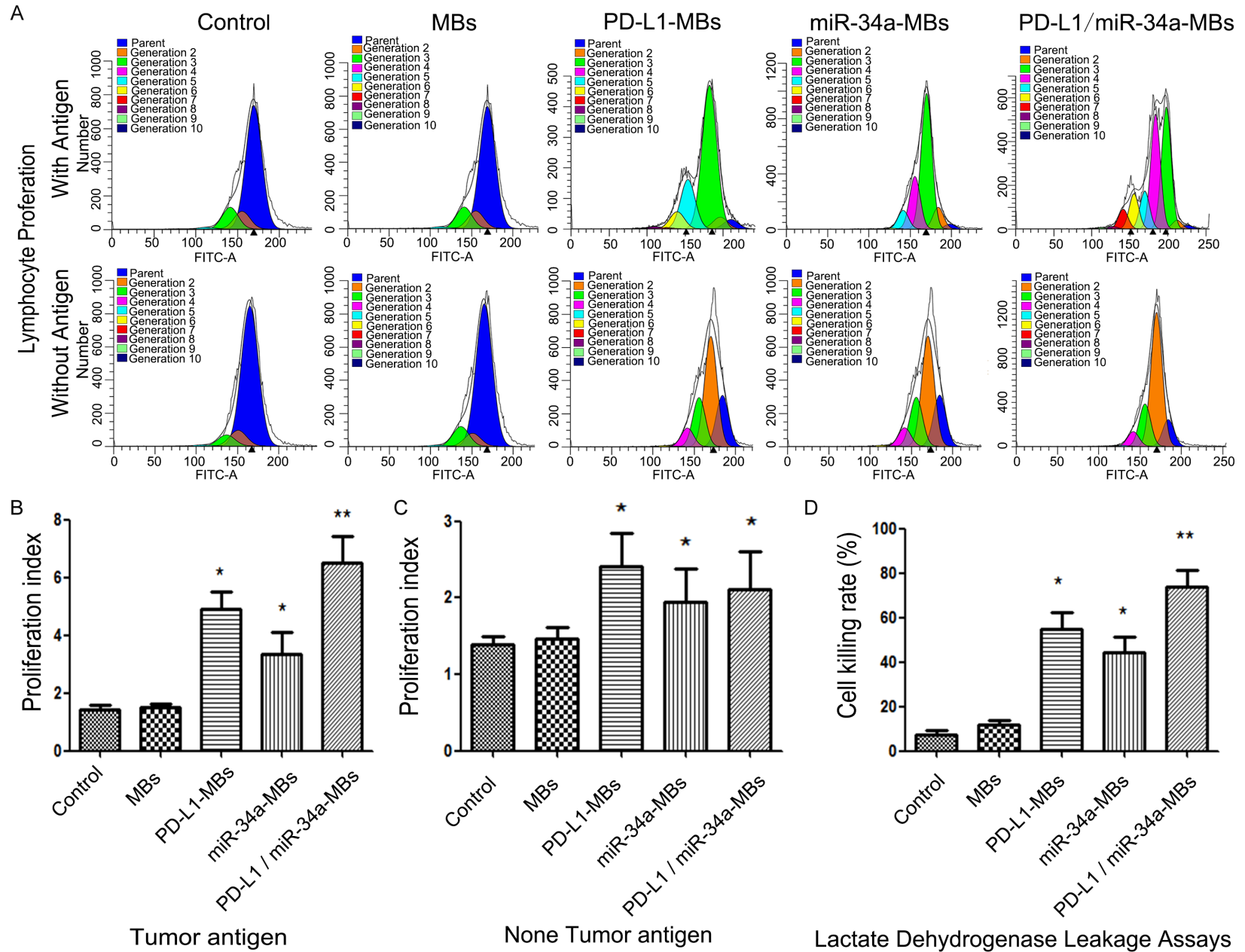
Figure 8. Analysis of the spleen lymphocyte proliferation after the targeted microbubbles by flow cytometry. A. Splenocytes were labeled with CFSE and cultured for 72 (with or without tumor antigen stimulation). B. Calculated the lymphocyte proliferation index in each group with tumor antigen; C. Calculated the lymphocyte proliferation index in each group without tumor antigen. D. The cytotoxicity of lymphocytes detected by Lactate dehydrogenase leakage assays, the cytotoxic cell killing rate increased significant in PD-L1 Ab-MBs + US group and miR-34a-MBs + US group, and the increasing of cytotoxic cell killing rate was more significant in PD-L1 Ab/miR-34a-MBs + US group. (Compared with the control group, *$P<0.05$, **$P<0.01$, n = 5).

effect [19]. US-triggered microbubbles destruction initiates a series of biochemical and physical reaction which augmented the permeability of physiological barriers, so that immunostimulatory factors can be allowed to pass across the barriers and exert their effects. Previous studies observed that low-frequency US combined with microbubbles promotes maturation and differentiation of dendritic cells (DCs) simultaneously in the cancer microenvironment [20]. And this variation could promote T lymphocytes mediated antitumor immunity regulation [21]. Meanwhile, the key point of cancer immunotherapies is to stimulate T-cell responses to tumor cell [22]. The most elucidated mechanism for tumor evasion of T cell-mediated immunity was the programmed cell death protein-1/programmed death-ligand 1 (PD-1/PD-L1) signaling axis [23]. PD-1, as a protein receptor, expressed in multiple immune cells, such as B cells, T cells, dendritic cells, monocytes and NK cells [24]. PD-L1, is the ligand to PD-1, which expressed on cancer cells, its overexpression has a great effect on suppress host immune response. When PD-L1 binds to PD-L1, it leads to a functional suppression of tumor infiltrating lymphocytes (TIL) and T cells. With using the antagonists of PD-1/PD-L1 signaling, it can partially reverse the exhaustion of T cells, and also can improve the function of T-cell mediated tumor immune regulation. Therefore, the PD-1 pathway is an important immune checkpoint to active and regulate the function of T cells and TIL [25-27]. In order to activate the antitumor immune system by blocking PD-1/PD-L1 signaling pathways, we developed PD-L1 antibody loaded MBs. These targeted MBs had a higher targeting efficiency bind to U14 cells. The experiment demonstrated that ultrasound mediated PD-L1 Ab-MBs, PD-L1 Ab/miR-34a-MBs could regulate immune function, ultrasound mediated targeted MBs binding to tumor cell with PD-L1 antibody, then through blocking PD-1/PD-L1 signaling pathways, activate the body's immune system, promote the effect of the activation of

T lymphocytes proliferation, increased infiltration of CD8+ T cells in the tumor tissue, promote the activity of immune cell factors (TNF-α and INF-γ) secretion, enhance antitumor immune killing effect.

With improved understanding of molecular mechanism in tumor proliferation and progression, the gene-targeted therapy for cancers was considered as a promising treatment for cancer. MicroRNAs (miRs) is a kind of small non-coding RNA molecules, which has important impact on cell proliferation, differentiation and apoptosis, and even can lead to tumor progression when the expression of miRs is abnormal [28]. The dysregulation of miR-34 family member exists in various tumors including cervical cancer. And miR-34 family has the function of anti-proliferative and pro-apoptotic, meanwhile, it can be regard a direct targets of p53. Specifically, miR-34a was considered to be the most characterized and special family member is located in the second exon of its main transcript [29, 30]. And it has been reported that, the expression of miR-34 family is downregulated in HPV-positive cells, it may induce the unstable of p53 and lead to proliferation of tumor cells [31]. The research of Wang and his colleages also proved this point, they found the expression of miR-34a was down-regulated significant compare to control group in cervical cancer patients' serum and tumor tissues [32]. Conversely, overexpression of miR-34a may induce cell-cycle arrest, inducing cell proliferation, apoptosis and even immune regulation [9]. With a deeper understanding of the expression of miR-34a is closely related to the occurrence and progression of cancer, MiR-34a was attempted to serve as a key biomarkers or targets for anticancer therapy [33]. In this study we tried to prepare the miR-34a microbubbles and delivery them to cervical cancer. Compared to control group, loaded miR-34a microbubbles had obviously promoted apoptosis on tumor cells and more positive apoptotic cells appeared as compared to control group. What's more, the results of

H&E staining revealed that a large part of necrotic area without cell structure were observed, apoptotic bodies were appeared but karyokinesis were rarely observed. These changings were lying on following reasons: Firstly, miR-34a-MBs and PD-L1 Ab/miR-34a-MBs could effectively penetrate to tumor cells and enter to extracellular matrix, which can enhance the delivery of miR-34a into deep of tumor with ultrasound irradiation in tumor region. Furthermore, overexpression and aggregation of miR-34a induced the stagnation of cervical cancer cell cycle and inhibited the proliferation of cervical cancer cells through up-regulating the expression of pro-apoptotic protein Bax and down-regulating the level of anti-apoptotic protein Bcl-2. As a result, it achieved a good therapeutic effect in this research.

It has been reported that systemic co-administration is more effective than monotherapy [34]. This study aims to combine anti-PD-L1 antibody with miR-34a, which combination immune therapy and gene therapy showed a valuable approach to systemic treatment for cervical cancer. These findings demonstrate that PD-L1 Ab/miR-34a-MBs + US treatment caused more obviously cell apoptosis and enhanced the immune response against the tumor progression. There is two main factors to explain this phenomenon. Firstly, PD-L1 Ab/miR-34a-MBs can bind to tumor cell with PD-L1 antibody, then through blocking PD-1/PD-L1 signaling pathways, activate the body's immune system, promote the effect of the activation of T lymphocytes proliferation. Secondly, the PD-L1 Ab/miR-34a-MBs + US group had a better targeting effect on cervical cancer tissues than the miR-34a-MBs + US group, owing to PD-L1 antibody bind to tumor cell, this targeted MBs could gather miR-34a with high-concentration aggregation and releasing around the cervical cancer, which could augment the gene quantity reached to the specific sites and improve the uptake of miR-34a by cervical cancer cells, thus, promoted the apoptosis of cancer cells. Co-delivery of antibody and genes with MB vectors can be a promising way to enhance anticancer effects was proved by this research.

Conclusion

In conclusion, PD-L1 Ab/miR-34a-MBs combined with US has been confirmed have a bet-

ter targeting and synergistic inhibition on cervical cancer. Using ultrasonic microbubbles as the carrier of antibodies and genes can improve the targeted uptake of therapeutic drugs at the lesion site and promote the effective transfection of genes. Multiple targeted microbubbles have better targeting ability to tumor tissues, improve the antibodies and genes concentration around tumor tissues, and reduce the systemic toxicity and side effects.

Disclosure of conflict of interest

None.

Address correspondence to: Dr. Qing Zhou, Department of Ultrasound Imaging, Renmin Hospital of Wuhan University, No. 238, Jiefang Road, Wuhan 430060, China. Tel: +86-027-88041911; Fax: +86-027-88041911; E-mail: qingzhou.wh.edu@hotmail.com; Dr. Yun Zhao, Medical College of China Three Gorges University, No. 8 Daxue Road, Xiling District, Yichang 443002, China. Tel: +86-0717-6397328; Fax: +86-0717-6397328; E-mail: ZY_zhaoyun123@163.com

References

[1] Bray F, Ferlay J, Soerjomataram I, Siegel RL, Torre LA and Jemal A. Global cancer statistics 2018: GLOBOCAN estimates of incidence and mortality worldwide for 36 cancers in 185 countries. CA Cancer J Clin 2018; 68: 394-424.
[2] Couzin-Frankel J. Breakthrough of the year 2013. Cancer immunotherapy. Science 2013; 342: 1432-1433.
[3] Ribas A and Wolchok JD. Cancer immunotherapy using checkpoint blockade. Science 2018; 1350-1355.
[4] Fesnak AD, June CH and Levine BL. Engineered T cells: the promise and challenges of cancer immunotherapy. Nat Rev Cancer 2016; 16: 566-581.

[5] Tipanee J, Chai YC, VandenDriessche T and Chuah MK. Preclinical and clinical advances in transposon-based gene therapy. Biosci Rep 2017; 37: BSR20160614.

[6] Wang TY, Choe JW, Pu KY, Devulapally R, Bachawal S, Machtaler S, Chowdhury SM, Luong R, Tian L, Khuri-Yakub B, Rao JH, Paulmurugan R and Willmann JK. Ultrasound-guided delivery of microRNA loaded nanoparticles into cancer. J Control Release 2015; 203: 99-108.

[7] Wang P, Yin T, Li J, Zheng B, Wang X, Wang Y, Zheng J, Zheng R and Shuai X. Ultrasound-responsive microbubbles for sonographyguided siRNA delivery. Nanomedicine 2016; 12: 1139-1149.

[8] Ding J, Mooers BH, Zhang Z, Kale J, Falcone D, McNichol J, Huang B, Zhang XC, Xing C, Andrews DW and Lin J. After embedding in membranes antiapoptotic Bcl-XL protein binds both Bcl-2 homology region 3 and Helix 1 of proapoptotic bax protein to inhibit apoptotic mitochondrial permeabilization. J Biol Chem 2014; 11873-11896.

[9] Zhang R, Su J, Xue SL, Yang H, Ju LL, Ji Y, Wu KH, Zhang YW, Zhang YX, Hu JF and Yu MM. HPV E6/p53 mediated down-regulation of miR-34a inhibits warburg effect through targeting LDHA in cervical cancer. Am J Cancer Res 2016; 6: 312-320.

[10] Kumari P, Ghosh B and Biswas S. Nanocarriers for cancer-targeted drug delivery. J Drug Target 2016; 179-191.

[11] Wu J and Nyborg WL. Ultrasound, cavitation bubbles and their interaction with cells. Adv Drug Deliv Rev 2008; 60: 1103-1116.

[12] Glasgow MD and Chougule MB. Recent developments in active tumor targeted multifunctional nanoparticles for combination chemotherapy in cancer treatment and imaging. J Biomed Nanotechnol 2015; 11: 1859-1898.

[13] Luo MH, Yeh CK, Situ B, Yu JS, Li BC and Chen ZY. Microbubbles: a novel strategy for chemotherapy. Curr Pharm Des 2017; 23: 3383-3390.

[14] Yang Q, Nanayakkara GK, Drummer C, Sun Y, Johnson C, Cueto R, Fu H, Shao Y, Wang L, Yang WY, Tang P, Liu LW, Ge S, Zhou XD, Khan M, Wang H and Yang X. Low-intensity ultrasound induced anti-inflammatory effects are mediated by several new mechanisms including gene induction, immunosuppressor cell promotion, and enhancement of exosome biogenesis and docking. Front Physiol 2017; 8: 818.

[15] Pysz MA, Machtaler SB, Seeley ES, Lee JJ, Brentnall TA, Rosenberg J, Tranquart F and Willmann JK. Vascular endothelial growth factor receptor type 2-targeted contrast-enhanced US of pancreatic cancer neovasculature in a genetically engineered mouse model: potential for earlier detection. Radiology 2015; 274: 790-799.

[16] Wu S, He X, Li M, Shi F, Wu D, Pan M, Guo M, Zhang R, Luo S, Gu N and Dou J. MiRNA-34a overexpression inhibits multiple myeloma cancer stem cell growth in mice by suppressing TGIF2. Am J Transl Res 2016; 8: 5433-5443.

[17] Yu J, Zhao Y, Liu C, Hu B, Zhao M, Ma Y and Jiang J. Synergistic anti-tumor effect of paclitaxel and miR-34a combined with ultrasound microbubbles on cervical cancer in vivo and in vitro. Clin Transl Oncol 2020; 22: 60-69.

[18] Wang W, Xia X, Wu S, Guo M, Lie P and He J. Cancer immunotherapy: a need for peripheral immunodynamic monitoring. Am J Reprod Immunol 2018; 79: e12793.

[19] Escoffre JM, Deckers R, Bos C and Moonen C. Bubble-assisted ultrasound: application in immunotherapy and vaccination. Adv Exp Med Biol 2016; 880: 243-261.

[20] Zhu L, Zhao H, Zhou Z, Xia Y, Wang Z, Ran H, Li P and Ren J. Peptide-functionalized phase-transformation nanoparticles for low intensity focused ultrasound-assisted tumor imaging and therapy. Nano Lett 2018; 18: 1831-1841.

[21] Zhang W, Shou WD, Xu YJ, Bai WK and Hu B. Low-frequency ultrasound-induced VEGF suppression and synergy with dendritic cell-mediated anti-tumor immunity in murine prostate cancer cells in vitro. Sci Rep 2017; 7: 5778-5793.

[22] Miller JF and Sadelain M. The journey from discoveries in fundamental immunology to cancer immunotherapy. Cancer Cell 2015; 27: 439-449.

[23] Smahel M. PD-1/PD-L1 blockade therapy for tumors with downregulated MHC class I expression. Int J Mol Sci 2017; 18: 1331-1338.

[24] Sui H, Ma N, Wang Y, Li H, Liu X, Su Y and Yang J. Anti-PD-1/PD-L1 therapy for non-small-cell lung cancer: toward personalized medicine and combination strategies. J Immunol Res 2018; 2018: 6984948.

[25] Knutson KL, Karyampudi L, Lamichhane P and Preston C. Targeted immune therapy of ovarian cancer. Cancer Metastasis Rev 2015; 34: 53-74.

[26] McClanahan F, Hanna B, Miller S, Clear AJ, Lichter P, Gribben JG and Seiffert M. PD-L1 checkpoint blockade prevents immune dysfunction and leukemia development in a mouse model of chronic lymphocytic leukemia. Blood 2015; 126: 203-211.

[27] Chen L, Azuma T, Yu W, Zheng X, Luo L and Chen L. B7-H1 maintains the polyclonal T cell response by protecting dendritic cells from cy-

totoxic T lymphocyte destruction. Proc Natl Acad Sci U S A 2018; 115: 3126-3131.

[28] Li S, Yang F, Wang M, Cao W and Yang Z. miR-378 functions as an onco-miRNA by targeting the ST7L/Wnt/β-catenin pathway in cervical cancer. Int J Mol Med 2017; 40: 1047-1056.

[29] Kumamoto K, Spillare EA, Fujita K, Horikawa I, Yamashita T, Appella E, Nagashima M, Takenoshita S, Yokota J and Harris CC. Nutlin-3a activates p53 to both down-regulate inhibitor of growth 2 and up-regulate mir-34a, mir-34b, and mir-34c expression, and induce senescence. Cancer Res 2008; 68: 3193-3203.

[30] Chang TC, Wentzel EA, Kent OA, Ramachandran K, Mullendore M, Lee KH, Feldmann G, Yamakuchi M, Ferlito M, Lowenstein CJ, Arking DE, Beer MA, Maitra A and Mendell JT. Transactivation of miR-34a by p53 broadly influences gene expression and promotes apoptosis. Mol Cell 2007; 26: 745-752.

[31] Wang X, Wang HK, McCoy JP, Banerjee NS, Rader JS, Broker TR, Meyers C, Chow LT and Zheng ZM. Oncogenic HPV infection interrupts the expression of tumor-suppressive miR-34a through viral oncoprotein E6. RNA 2009; 15: 637-647.

[32] Wang P, Zhai G and Bai Y. Values of miR-34a and miR-218 expression in the diagnosis of cervical cancer and the prediction of prognosis. Oncol Lett 2018; 15: 3580-3585.

[33] Córdova-Rivas S, Fraire-Soto I, Mercado-Casas Torres A, Servín-González LS, Granados-López AJ, López-Hernández Y, Reyes-Estrada CA, Gutiérrez-Hernández R, Castañeda-Delgado JE, Ramírez-Hernández L, Varela-Silva JA and López JA. 5p and 3p strands of mir-34 family members have differential effects in cell proliferation, migration, and invasion in cervical cancer cells. Int J Mol Sci 2019; 20: 545.

[34] Zhang L, Yang X, Lv Y, Xin X, Qin C, Han X, Yang L, He W and Yin L. Cytosolic co-delivery of miRNA-34a and docetaxel with core-shell nanocarriers via caveolae-mediated pathway for the treatment of metastatic breast cancer. Sci Rep 2017; 7: 46186.